

Scene Adaptive Structured Light 3D Imaging

Tomislav Pribanic¹^a, Tomislav Petkovic¹^b, David Bojanic¹^c, Kristijan Bartol¹^d
and Mohit Gupta²

¹Faculty of Electrical Engineering and Computing, University of Zagreb, Unska 3, Zagreb, Croatia

²Department of Computer Science, University of Wisconsin, Madison, WI, U.S.A.

Keywords: 3D Imaging, Structured Light, Time-of-Flight, Depth Precision.


Abstract: A 3D structured light (SL) system is one powerful 3D imaging alternative which in the simplest case is composed of a single camera and a single projector. The performance of 3D SL system has been studied considering many aspects, for example, accuracy and precision, robustness to various imaging factors, applicability to a dynamic scene capture, hardware and image processing complexity, to name but a few. In this work we consider the spatial projector-camera set up and its influence on the uncertainty of points' depth reconstruction. In particular, we show how a depth precision is in a great extent determined by the angle of pattern projection and the angle of imaging from a projector and a camera, respectively. For a fixed camera projector configuration, those angles are scene dependent for various points in space. Consequently, the attainable depth precision will typically vary considerably across the volume of reconstruction which is not a desirable property. To that end, we study a scene dependent 3D imaging approach during which we propose how to conveniently detect points with a lower depth precision and to influence other factors of a depth precision, in order to improve a depth precision in scene parts where necessary.


1 INTRODUCTION


The study on 3D imaging system design has attracted a great deal of attention in computer vision. There has been many methods and systems proposed (Chen, Brown, & Song, 2000). A particularly interesting ones are active illumination 3D imaging systems where, besides a camera, an active source of illumination is introduced. The most representative ones are photometric systems (Barsky & Maria, 2003), time-of-flight (ToF) cameras (Hansard, Lee, Choi, & Horaud, 2012) and structured light (SL) systems (Geng, 2011). SL has proven to be one of the most accurate and robust methods proposed and analyzed (Salvi, Fernandez, Pribanic, & Xavier, 2010). In SL an illumination source is typically a projector. The main task of a projector is to project pattern(s) in the scene. That is especially beneficial when a natural scene has a low texture since SL is triangulation-based 3D imaging system and, in order to triangulate 3D point position, it is necessary to find


the correspondent projector and camera image coordinates. Having basically two different pieces of hardware HW, i.e. a camera and a projector, opened an additional vast amount of research possibilities to study the performance of SL systems. Naturally, the reconstruction accuracy and precision aspects have been given perhaps the most attention. To that end, different factors and system design issues have been analyzed and various measures have been proposed in order to improve the accuracy and precision. However, somewhat surprisingly and to the best of our knowledge, there is relatively less work about the spatial geometrical set up between a camera and a projector (Liu & Li, 2014). We note that besides a camera projector baseline, two other most obvious factors defining a geometry of 3D reconstruction are the angle of projector's pattern projection and the angle of camera imaging (angles α and β in Figure 1).

In this work our main contributions are related to those two angles and to their influence on the depth precision. First, we derive an expression clearly

^a <https://orcid.org/0000-0002-5415-3630>

^b <https://orcid.org/0000-0002-3054-002X>

^c <https://orcid.org/0000-0002-2400-0625>

^d <https://orcid.org/0000-0003-2806-5140>

showing the various factors determining the depth precision of a SL system, two of which are the aforementioned angles of pattern projection and imaging. We further demonstrate how those two angles change across the scene, thus having a significant impact on the expected depth precision throughout the scene. Obviously, the pair of such angles are scene dependent and for a general scene cannot be anticipated in advance. We also provide a simple measure on improving the depth precision for those points in space where the particular angles cause an unsatisfactory depth precision. In turn, the proposed strategy allows scene dependent 3D imaging.

The remainder of this work is structured as follows. We next briefly cover the related work on 3D active imaging. Afterwards we derive an expression for SL system depth precision, followed by the experimental simulations of depth precision dependency on angles of pattern projection and imaging. In the same section we discuss possible measures of improving the depth precision. At the end we reflect on the possible future work and draw the main paper conclusions.

2 RELATED WORK

A common approach to classify 3D imaging systems is to divide them in the following three groups: triangulation, interferometry and time-of flight (Büttgen, Oggier, Lehmann, Kaufmann, & Lustenberger, 2015). An even simpler classification would be only in two groups: passive and active 3D imaging systems. Within the active ones two most notable representatives, and closely related to this work, are structured light systems and time of flight cameras which will be, therefore, in brief jointly overviewed.

Due to a fact that an active source of illumination has been utilized, a significant deal of work was devoted to the performance error analyses where multiple illuminations sources (3D imaging systems) are simultaneously used. To prevent either interfering one SL projector with another or one ToF LED (laser) source with another several approaches have been proposed: space division-multiple access (Jia, Wang, Zhou, & Meng, 2016), wavelength-division multiple access (Bernhard & Peter, 2008), time-division multiple access, frequency-division multiple access) (Petković, Pribanić, & Đonlić, 2017), and finally, in the case of ToFs, a code-division multiple access (Whyte, Payne, Dorrington, & Cree, 2010).

When analyzing the performance of a single 3D imaging system, a significant work was done, mostly in the field of ToFs, studying hardware itself w.r.t. to various factors such as power budget, quantum noise and thermal noise (Lange & Seitz, 2001); or integration time related error and built-in pixel related error (Foix, Alenya, & Torras, 2011). On the other hand, SL system performance has been analyzed mainly in the hardware agnostic manner, i.e. more in the image processing sense by trying to identify potential errors during pattern(s) (de)coding process (Horn & Kiryati, 1997) and/or by finding the optimal coding scheme (Gupta & Nakhate, A Geometric Perspective on Structured Light Coding, 2018). That is in a way understandable since in terms of signal processing ToF is generally based on two or three principles: continuous/discrete and direct time of flight (Horaud, Hansard, Evangelidis, & Ménier, 2016). On the other hand, SL has richer alternatives regarding the various types of patterns to be projected and subsequently processed, particularly using color patterns for dynamic scenarios (Petković, Pribanić, & Đonlić, 2016). In that sense a high emphasis was put on a design of patterns to be projected (Mirdehghan, Chen, & Kutulakos, 2018). Interestingly, certain hardware design proposed solutions for ToF, e.g. epipolar time of flight imaging (Achar, Bartels, Whittaker, Kutulakos, & Narasimhan, 2017), are applicable for SL too.

One of the main differences between ToF and SL is the former does not have the baseline involved since ToF illumination source and camera are generally assumed to be collocated. In terms of the baseline, an interesting work has been done in SL when the baseline is very small which simplifies the process of finding a projected code in cameras images (Saragadam, Wang, Gupta, & Nayar, 2019). Moreover, a close work to ours is the one analyzing the influence of the short projector-camera baseline on the performance (Liu & Li, 2014). Similarly (Bouquet, Thorstensen, Bakke, & Risholm, 2017) compares the performance 3D SL and ToF systems, but without any relation to the geometrical configuration between the camera and the projector. To the best of our knowledge none of the mentioned works are specially concentrated on the analyses of the pattern projection angle and the camera imaging angle and their impact on the estimated depth precision.

3 DEPTH PRECISION OF SL 3D IMAGING SYSTEM

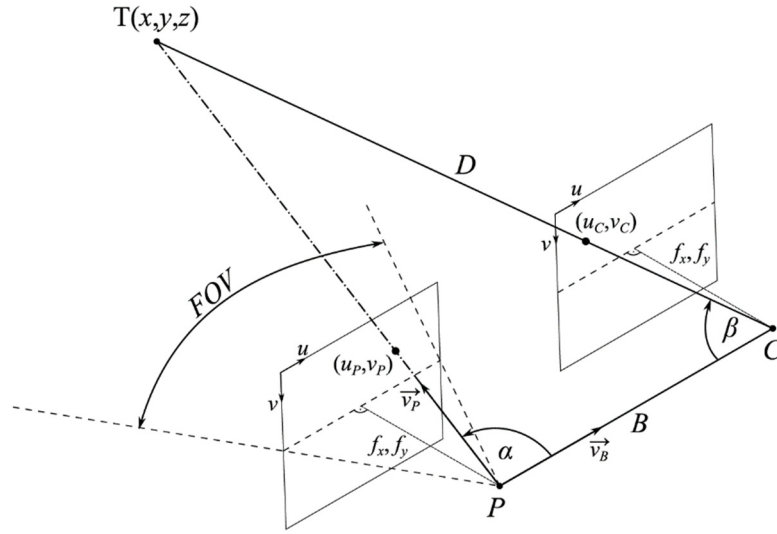


Figure 1 A: 3D point T , at the depth D from the camera (C), is projected in the camera (C) image at (u_c, v_c) and in the projector (P) image at (u_p, v_p) . Backprojected rays to the point T from the projector and the camera form with the baseline B the angles α and β , respectively. FOV stands for a projector's field of view. f_x and f_y are the effective focal lengths in the horizontal and vertical direction, respectively.

We start by introducing the basic principle behind phase shifting (PS) method which is very likely the most notable SL pattern strategy (Salvi, Fernandez, Pribanic, & Xavier, 2010). PS consists of sequentially projecting a number ($N \geq 3$) of periodic sine patterns, shifted by some phase shift $\varphi_i = \frac{2\pi}{N} \cdot i$, where $i=0, 1, \dots, N-1$. The projected patterns are imaged by a camera and then processed to compute a wrapped phase φ , based on which the correspondence between projector and camera image pixels can be established. The intensity I_i observed at some camera pixel can be modeled as follows:

$$I_i = A \cdot \sin(\varphi + \varphi_i) + C \quad (1)$$

where A is the brightness when projector projects its full intensity (A is related to 3D points reflectivity and propagation loss), φ is the unknown phase, φ_i is the known relative phase shift at which a particular pattern was projected, and C represents the contribution from a background illumination. Evidently having three unknowns (A , φ and C) there are at least $N=3$ shifts (projected patterns) needed to recover all three unknowns. In practice to cope with the noise at least four shifts are normally used, both in SL and ToF systems also (Büttgen, Oggier, Lehmann, Kaufmann, & Lustenberger, 2015), which allows to recover the unknowns:

$$\begin{aligned} A &= \frac{\sqrt{(I_0 - I_2)^2 + (I_1 - I_3)^2}}{2} \\ \varphi &= \tan^{-1} \left(\frac{I_0 - I_2}{I_1 - I_3} \right) \\ C &= \frac{I_0 + I_1 + I_2 + I_3}{4} \end{aligned} \quad (2)$$

We next derive a depth precision of the SL system. Figure shows rectified, but still a very general relationship between a projector, a camera and some triangulated point in space. Using the law of sines, we derive an expression for the depth D :

$$D = \frac{B \cdot \sin(\alpha)}{\sin(\alpha + \beta)} \quad (3)$$

where B is projector-camera baseline, and given some point T , α is projector pattern projection angle with the respect to baseline B and β is a camera imaging angle with the respect to baseline B too. Depth precision can be quantitatively estimated as a depth uncertainty where the cause of uncertainty can be attributed to the noise in measurements I_i of Eq. (1). In particular, a standard deviation σ_D of depth is commonly estimated using the expression for the error propagation:

$$\sigma_D = \sqrt{\sum_{i=0}^{N-1} \left(\frac{\partial D}{\partial I_i}\right)^2 \cdot \text{Var}(I_i)} \quad (4)$$

where the variance $\text{Var}(I_i)$ is modeled as being equal to the signal level (Lange & Seitz, 2001). According to the expression (3), the depth D is explicitly dependent on the angles α and β . However, angle α can be expressed as a function of the phase φ (2) which in turn provides a relationship to the measurements I_i . Hence, using the chain rule the partial derivative $\frac{\partial D}{\partial I_i}$ can be expressed as:

$$\frac{\partial D}{\partial I_i} = \frac{\partial D}{\partial \alpha} \cdot \frac{\partial \alpha}{\partial \varphi} \cdot \frac{\partial \varphi}{\partial I_i} \quad (5)$$

Based on Eq. (3), the first factor in Eq. (5) is readily computed:

$$\frac{\partial D}{\partial \alpha} = \frac{B \cdot \sin \beta}{\sin^2(\alpha + \beta)} \quad (6)$$

The actual relationship between the angle α and the phase φ is less obvious. According to Figure 1, the vector v_p pointing back in space in the direction of the spatial point T can be computed based on the projector calibration matrix K_p and on the projector image point $p=[u_p \ v_p \ 1]^T$:

$$K_p = \begin{bmatrix} f_x & 0 & u_0 \\ 0 & f_y & v_0 \\ 0 & 0 & 1 \end{bmatrix} \quad (7)$$

$$v_p = K_p^{-1} \cdot p = \begin{bmatrix} u_p - u_0 \\ f_x \\ v_p - v_0 \\ f_y \\ 1 \end{bmatrix}_p$$

where (u_p, v_p) are projector image coordinates, (u_0, v_0) is the position of the principal point in the projector image. f_x and f_y are effective focal lengths in horizontal and vertical direction, respectively. For the simplicity of exposition and without loss of generality we can set an image component coordinate u as being identical to the wrapped phase φ . Next, the angle α is immediately determined by a dot product between the vector v_p and the baseline B direction vector v_B , where v_B can be taken as a unit vector.

$$\cos \alpha = \frac{\text{dot}(v_p, v_B)}{|v_p| \cdot |v_B|} = \frac{\text{dot}(v_p, v_B)}{|v_p|} \quad (8)$$

Evidently this poses a nonlinear relationship between the angle α and the wrapped phase φ . Fortunately, the angle α typically spans values where the $\cos \alpha$ is fairly linear w.r.t. its argument (unless a wide-angle optics for a projector is used). Therefore, similarly as

in (Bouquet, Thorstensen, Bakke, & Risholm, 2017), we approximate the relationship between the angle α and the wrapped phase φ with a linear function. Using fairly straightforward geometry relations, depicted on Figure , it can be shown that:

$$\alpha \approx -\text{FOV}/\varphi_{\text{MAX}} \cdot \varphi + \frac{\pi + \text{FOV}}{2} \quad (9)$$

where FOV is projector's field of view. Eq. (9) finally determines the partial derivative $\frac{\partial \alpha}{\partial \varphi} = -\frac{\text{FOV}}{\varphi_{\text{MAX}}}$ and simplifies the original (4) to.

$$\sigma_D = \frac{B \cdot \sin \beta \cdot \text{FOV}}{\sin^2(\alpha + \beta) \cdot \varphi_{\text{MAX}}} \cdot \sqrt{\sum_{i=0}^{N-1} \left(\frac{\partial \varphi}{\partial I_i}\right)^2 \cdot I_i} \quad (10)$$

The sum of partial derivatives under the square root from (10), using the relations (1) and (2), will yield $\frac{\sqrt{C}}{\sqrt{2 \cdot A}}$ and will ultimately define the final expression for the depth standard deviation σ_D :

$$\sigma_D = \frac{D^2 \cdot \text{FOV} \cdot \sqrt{C}}{B \cdot \varphi_{\text{MAX}} \cdot \sqrt{2} \cdot A} \cdot \frac{\sin \beta}{\sin^2 \alpha} \quad (11)$$

$$\sigma_D = \frac{B \cdot \text{FOV} \cdot \sqrt{C}}{\varphi_{\text{MAX}} \cdot \sqrt{2} \cdot A} \cdot \frac{\sin \beta}{\sin^2(\alpha + \beta)}$$

Here we point out the dependence of σ_D on the part we call the angle factor $AF = \frac{\sin \beta}{\sin^2(\alpha + \beta)}$. In the next section we show how AF affects the amount of standard deviation σ_D across the reconstruction whole volume.

4 RESULTS AND DISCUSSION

In this section we first show how the angle factor AF varies across a 3D imaging scene. Then we use Monte Carlo approach in the synthetic experiments to estimate the depth standard variation σ_D for various points in the 3D space. Finally we propose and discuss strategies to improve depth precision for the desired portion of space, in order to achieve a more uniform depth precision values across the volume. To that end, and without loss of generality, we assume one plausible projector-camera set up where projector and camera images are epipolarly rectified (Fusiello, Trucco, & Verri, 2000) and with the following parameters: the baseline $B=300\text{mm}$, the effective focal lengths in pixels $f_x=f_y=1000$, image resolution

$(u, v)=(1024, 768)$, the principal point coordinates $(u_0, v_0)=(512, 384)$.

Figure 2 visualizes the change of AF for a given volume and at the standoff distance 400mm from the 3D SL scanner. In the case of this rectified projector-camera set up, AF factor increases (a depth precision becomes worse) almost linearly along the volume depth. However, besides volume depth alone, which can be fairly arbitrary defined, we are even more interested about AF dependency of the depth D wrt to the camera itself.

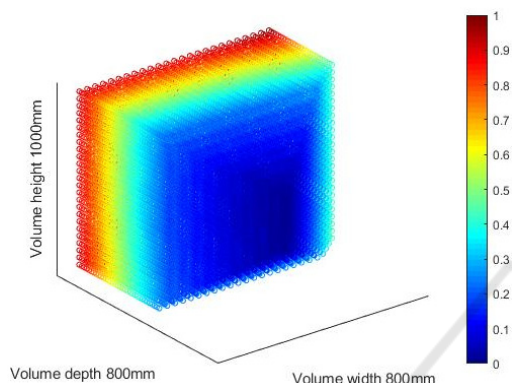


Figure 2: The relative change of AF across the 3D imaging volume $800\text{mm}\times 800\text{mm}\times 1000\text{mm}$ (width \times depth \times height). 3D scanner standoff distance is 400mm.

Figure 3 shows, for a sequence of constant depths D , how AF changes as the angle α changes, spanning the entire projector’s FOV angle. Given the current projector-camera arrangement it turns out that at some constant depth D , AFs become worse and worse as the angle α increases. In fact, the relative discrepancy between points having a small AF and points having a big AF is more evident as the depth D is smaller.

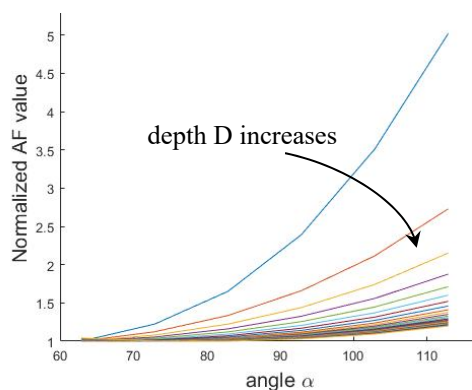


Figure 3: Each solid curve corresponds to a constant depth. Going from the top curve to the bottom, depth D changes from 350mm to 1000mm. Values within each curve are normalized on the smallest AF value for that curve (depth).

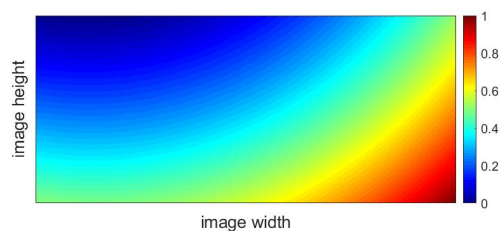


Figure 4: A camera image of the 3D plane of points, parallel to the projector-camera image plane, where the intensity represents the values of AF.

Figure 4 presents another alternative overlook on the issue. In this case points in 3D plane, at the standoff distance of about 300mm and parallel to the projector-camera image planes, are projected to the camera image where for each point the value AF is shown as the intensity. Going from the upper left corner to the lower right corner, a diversity of AF values is witnessed, even though the points are in the plane parallel to the projector/camera images. Thus, one must not conclude, as may seem at the first glance based solely on the previous Figure 2, that in planes parallel to the projector-camera image plane there are no notable changes in the AF values. Therefore, in the case of a general scene it is reasonable to expect points having different values for the angles α and β not only at different depths D , but also within the same depth D as well. In turn, a diverse set of AF values is expected to be present. The fact is that having point clouds reconstructed with the significantly different precision values per individual points may impair further processing on the point cloud itself.

The natural question raises on how to improve the depth precision for a desired portion of 3D points or even for individual points. Examining the expression (11) we notice the depth standard variation σ_D is controlled by several parameters. The one most convenient to control is likely to be the value A dictated by the strength of the illumination source. Using the illumination source with an adjustable illumination power over different portion of projector images/patterns, such as in (Gupta, Yin, & Nayar, Structured Light In Sunlight, 2013), it is possible to relatively easily decrease or increase the value of A during the scanning (pattern projection). In turn this assures a seamless approach to directly impact the depth standard variation σ_D in the areas where needed. Our proposed approach initially scans 3D scene simply to get an estimate on AF values. This initial scan is done in practice using the fewest number of patterns possible since we just need a rough estimate of AF values which does not require highly accurate and precise 3D reconstruction. Afterward, the scene

is re-scanned using the full set of patterns and with the appropriate strengths of the illuminations across the scene.

In attempt to verify the crucial part of our approach we perform the following simulation. We randomly sample $M=100$ points from the volume as defined in Figure 2. Such point set will exhibit a significantly different AF values. For each of these 3D points we estimate the depth standard variation σ_D using the Monte Carlo simulation. That is, we assume an additive Gaussian noise on the image values I_i from Eq.(1), with noise variance equal to I_i , and generate such random noise values in order to compute the phase φ from Eq.(2). Knowing φ we can eventually estimate noisy depth D . Repeating the experiment a number of times ($N=10000$) for each known 3D point, allows us to estimate directly the depth standard deviation σ_D . According to our theory we expect to see a proportional relation between the estimated depth standard deviation and the corresponding AF of a certain point. In another words, the ratios between the different depth standard deviations σ_D should be the same as the ratios of AF 's. Following the above-mentioned simulation, Figure 5 presents on the vertical axis the estimated depth standard deviations normalized to the smallest one in the randomly chosen set of the above mentioned $M=100$ points. On the horizontal axis the corresponding AF 's are normalized to the AF of the smallest estimated depth standard deviation. In Figure 5 emerges (almost) a straight diagonal (red) line which confirms our predicted theory.

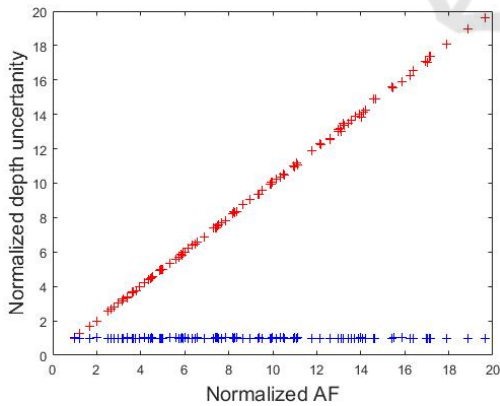


Figure 5: Diagonal (red) line: Verification of the relationship between the depth precision and AF . Horizontal (blue) line: After the proposed adjustment of illuminations source strength, depth precision becomes invariant w.r.t. AF .

Next, we look for the ratio of AF 's with the respect to the point having the smallest (within

randomly chosen set of $M=100$ points) estimated depth standard deviation and we aim to appropriately increase the illuminations strength of all other points in order to achieve the same depth precision. Thus, we run another Monte Carlo simulation for estimation of standard deviations, but this time with the suitably increased value A for each of the remaining points. Figure 5 shows a straight horizontal (blue) line proving that after the proposed adjustment of the illumination strength a depth precision (an estimated depth standard variation) is uniform across all 3D points, i.e. it is independent of the AF .

5 CONCLUSIONS

In this work we have proposed a method for scene dependent 3D imaging aimed at improving the depth precision at various 3D points in space. We have begun by developing a theoretical framework explaining the depth precision in 3D imaging system based on the SL principle. Within this framework we have identified several key factors determining a depth precision, among which are the projector's angle of pattern projection and the camera's angle of imaging. We have proposed to analyze jointly the influence of these two angles through a proposed angle factor AF . Having established a clear dependence of AF on the depth precision, we have further proposed a simple approach to improve the depth precision on the desired set of points, by manipulating the strength of the illumination source. The foreseen future work will include the implementation and evaluation using the actual hardware. In addition, we plan to consider the improvement of depth precision using other factors such as the number of phase shifts undertaken during the phase shifting procedure.

ACKNOWLEDGEMENTS

This work has been supported in part by Croatian Science Foundation under the project IP-2018-01-8118, in part by the European Regional Development Fund under the grant KK.01.1.1.01.0009 (DATACROSS) and in part by the Fulbright U.S. Visiting Scholar Program.

REFERENCES

- Achar, S., Bartels, J. R., Whittaker, W. L., Kutulakos, K. N., & Narasimhan, S. G. (2017). Epipolar time-of-flight imaging. *ACM Transactions on Graphics (TOG)*, 36(4), 371:1-37:8. doi:10.1145/3072959.3073686
- Barsky, S., & Maria, P. (2003). The 4-Source Photometric Stereo Technique for Three-Dimensional Surfaces in the Presence of Highlights and Shadows. *IEEE Transactions on Pattern Analysis and Machine Intelligence*, 25(10), 1239-1252.
- Bernhard, B., & Peter, S. (2008). Robust Optical Time-of-Flight Range Imaging Based on Smart Pixel Structures. *IEEE Transactions on Circuits and Systems I*, 55(6), 1512 - 1525.
- Bouquet, G., Thorstensen, J., Bakke, K. A., & Risholm, P. (2017). Design tool for TOF and SL based 3D cameras. *Optics Express*, 25(22), 27758-27769. doi:10.1364/OE.25.027758
- Büttgen, B., Oggier, T., Lehmann, M., Kaufmann, R., & Lustenberger, F. (2015). CCD/CMOS lock-in pixel for range imaging: Challenges, Limitations and State-of-the-Art. In *In Proceedings of 1st Range Imaging Research Day* (pp. 21-32).
- Chen, F., Brown, G., & Song, M. (2000). Overview of three-dimensional shape measurement using optical methods. *Optical Engineering*, 31(1), 10-22.
- Foix, S., Alenya, G., & Torras, C. (2011). Lock-in Time-of-Flight (ToF) Cameras: A Survey. 11(3), *IEEE Sensors Journal*. doi:10.1109/JSEN.2010.2101060
- Fusiello, A., Trucco, E., & Verri, A. (2000). A Compact Algorithm for Rectification of Stereo Pairs. *Machine Vision and Applications*, 12(1), 16-12. doi:doi.org/10.1007/s001380050
- Geng, J. (2011). Structured-light 3D surface imaging: a tutorial. *Advances in Optics and Photonics*, 3(2), 128-160. doi:doi.org/10.1364/AOP.3.000128
- Gupta, M., & Nakhate, N. (2018). A Geometric Perspective on Structured Light Coding. *European Conference on Computer Vision* (pp. 90-107). Munich: Springer, Cham. doi:10.1007/978-3-030-01270-0_6
- Gupta, M., Yin, Q., & Nayar, S. K. (2013). Structured Light In Sunlight. *IEEE International Conference on Computer Vision (ICCV)*, (pp. 1-8). Sydney.
- Hansard, M., Lee, S. L., Choi, O. C., & Horaud, R. (2012). *Time of Flight Cameras: Principles, Methods, and Applications*. London: Springer. doi:10.1007/978-1-4471-4658-2
- Horaud, R., Hansard, M., Evangelidis, G., & Ménéier, C. (2016). An Overview of Depth Cameras and Range Scanners Based on Time-of-Flight Technologies. (S. Verlag, Ed.) *Machine Vision and Applications*, 27(7), 1005-1020. doi:10.1007/s00138-016-0784-4
- Horn, E., & Kiryati, N. (1997). Toward optimal structured light patterns. *Proceedings. International Conference on Recent Advances in 3-D Digital Imaging and Modeling* (pp. 28-35). Ottawa: IEEE. doi:10.1109/IM.1997.603845
- Jia, T., Wang, B., Zhou, Z., & Meng, H. (2016). Scene depth perception based on omnidirectional structured light. *IEEE Transactions on Image Processing*, 25(9), 4369 - 4378. doi:10.1109/TIP.2016.2590304
- Lange, R., & Seitz, P. (2001). Solid-State Time-of-Flight Range Camera. *IEEE Journal of Quantum Electronics*, 37(3), 390-397. doi:10.1109/3.910448
- Liu, J., & Li, Y. (2014). Performance analysis of 3-D shape measurement algorithm with a short baseline projector-camera system. *Robotics and Biomimetics*, 1-10. doi:doi.org/10.1186/s40638-014-0001-8
- Mirdehghan, P., Chen, W., & Kutulakos, K. N. (2018). Optimal Structured Light a la Carte. *Computer Vision and Pattern Recognition (CVPR)*, (pp. 6248-6257). Salt Lake City. doi:10.1109/CVPR.2018.00654
- Petković, T., Pribanić, T., & Đonlić, M. (2016). Single-Shot Dense 3D Reconstruction Using Self-Equalizing De Bruijn Sequence. *IEEE Transactions on Image Processing*, 25(11), 5131-5144. doi:10.1109/TIP.2016.2603231
- Petković, T., Pribanić, T., & Đonlić, M. (2017). Efficient Separation between Projected Patterns for Multiple Projector 3D People Scanning. *International Conference on Computer Vision (ICCV): Workshop on Capturing and Modeling Human Bodies, Faces and Hands.*, (pp. 815-823). Venice.
- Salvi, J., Fernandez, S., Pribanic, T., & Xavier, L. (2010). A state of the art in structured light patterns for surface profilometry. *Pattern Recognition*, 43(8), 2666-2680. doi:doi.org/10.1016/j.patcog.2010.03.004
- Saragadam, V., Wang, J., Gupta, M., & Nayar, S. (2019). Micro-Baseline Structured Light. *International Conference on Computer Vision (ICCV)*, (str. 4049-4058). Seoul.
- Whyte, R. Z., Payne, A. D., Dorrington, A. A., & Cree, M. J. (2010). Multiple range imaging camera operation with minimal performance impact. *IS&T/SPIE Electronic Imaging*, 7538, pp. 75380I-1-10. San Jose. doi:10.1117/12.838271